Supporting Information

69451 Weinheim, Germany

Fast Exfoliation and Functionalisation of 2D Crystalline Carbon Nitride by Framework Charging

Jingjing Jia, Edward R. White, Adam J. Clancy, Noelia Rubio, Theo Suter, Thomas S. Miller, Paul F. McMillan, Veronika Brázdová, Furio Corà, Chris A. Howard, Robert V. Law, Cecilia Mattevi*, and Milo S. P. Shaffer*

Abstract: 2D layered graphitic carbon nitride nanosheets offer tunable electronic and chemical properties. However, exfoliation and functionalisation of gCN for specific applications remains challenging. We report a scalable one-pot reductive method to produce solutions of single and few layer 2D gCN nanosheets with excellent stability in a high mass yield (35%) from polytriazine imide. High resolution imaging confirms the intact crystalline structure and identifies an AB stacking. The first successful deliberate organic functionalisation of dissolved gCN is illustrated, providing a general route to adjust their properties.

DOI:

Experimental Procedures

1. Ionothermal synthesis of crystalline PTI:

Lithium bromide (LiBr, Aldrich) and potassium bromide (KBr, Alfa Aesar) eutectic mixture (52:48 wt%, Tm=329 ˚C) was prepared according to literature.[1] Dicyandiamide (DCDA, Sigma-Aldrich, 2g) was ground together with LiBr/KBr thoroughly in a glove box under N_2 atmosphere. The reaction mixture was heated in a tube furnace (Carbolite, MTF 12/38/250) at 10 ˚C·min^{-1} ramp rate to 400 ˚C for 6 h under N_2. After natural cooling to room temperature (RT), the resultant material was transferred back to the glove box and was loaded under nitrogen into a dried thick-walled quartz glass ampoule (Robson Scientific, Φ_{outer} = 23 mm, Φ_{inner} = 20 mm, length = 15 cm) which was evacuated to 10^{-6} mbar using a turbo pump (Leybold vaccum systems, PT70G compact). This ampoule was then sealed to form a static vacuum using an CH_4/O_2 flame, placed in a chamber furnace (Carbolite, CWF11/13) and heated to 600 ˚C at 10 ˚C·min^{-1} for 12 hours, before cooling to RT at ramp rate of 10 ˚C min^{-1}. The ampoule was carefully broken, and the PTI Li^+Br^- was recovered by washing the solidified salt block with distilled water several times, followed by several washes with ethanol (Millipore). The resulting material was then dried using a rotary evaporator (Buchi Rotavapour R-3, Vacuum pump V-700) to yield PTI Li^+Br^- as dark brown powder (~1.6 g).

Intercalants were removed from the PTI Li^+Br^- by hot water washing.[2] PTI Li^+Br^- (1.58 g) was loaded into a cellulose thimble (Whatman, Φ_{outer} = 27 mm, Φ_{inner} = 25 mm, length=80 mm), and placed into a Soxhlet extractor, where the reservoir was filled with distilled water and heated to reflux. After washing for 5 consecutive days, the material was recovered from the cellulose thimble, rinsed with ethanol, and then dried using a rotary evaporator. Crystalline PTI powders were recovered as brown powder (1.04 g, 66% yield).

2. Preparation of sodium naphthalide (NaNp)/DMAc solution:

Naphthalene was thoroughly dried in the presence of phosphorus pentoxide under vacuum overnight before transferring into the glove box (mBraun with N_2 atmosphere, both O_2 and water contents were less than 0.1 ppm). 1 $mg_{(Na)}$·mL^{-1} NaNp in DMAc was prepared following previous work,[3] where equimolar sodium (100 mg) and naphthalene (557 mg) were added to 100 mL DMAc and stirred overnight with a glass stirrer bar at RT in the glove box. All the chemicals are from Sigma-Aldrich.

3. PTI dissolution by framework charging method:

In a typical experiment, for example 1.4 mg·mL^{-1} initial PTI loading charged to a 7:1 PTI : Na molar ratio, PTI (28 mg, 2.13 mmol) were dried under vacuum (~10^{-1} mbar) with heating gun at 250 °C for 2 h, and kept under vacuum overnight before moving into the glove box. 7 mL (0.30 mmol) of 1 $mg_{(Na)}$·mL^{-1} NaNp/DMAc was diluted with 13 mL of DMAc and added to dried PTI. The mixture was stirred with a glass stirrer bar at ~250 rpm for several hours before pipetting into fluorinated ethylene propylene centrifuge tubes (Oak Ridge) with PTFE tape sealing the cap thread and centrifuged at 5000 *g* for 30 min before decanting in N_2 atmosphere to recover a solution of reduced PTI (FL-PTI^{n-}). Yield (the mass ratio of solubilised FL-PTI^{n-} nanosheets to the intial PTI) was measured by discharging of 20 mL solution by bubbling with dry air for 1 h before filtering over a tared 20 nm pore anodic aluminum oxide (AAO) membrane (Whatman) and washing with copious amounts of tetrahydrofuran (THF), ethanol, deionized water and acetone, ensuring the sample did not dry out between washings. The sample was subsequently dried at 60 ˚C for 48 h and weighed. A membrane subjected to the similar washing procedure using 20 mL DMAc substituting the PTI solution returned to the tared weight (± 0.1 mg). The PTI:Na molar ratio is defined as the number of C/N atoms within PTI framework per Na, supposing an average PTI M_w of 13.14 without considering a trace amount of residue intercalted Li^+.

4. Alkylation of solubilised PTI (FL-PTI^{n-}):

1-bromododecane ($C_{12}H_{25}Br$, Sigma-Aldrich) was degassed *via* freeze-pump-thaw method and dried with ~10 vol% activated 3 Å molecular sieves for at least 2 days before using. In a typical experiment, 0.13 mmol $C_{12}H_{25}Br$ (3 molar equivalent to Na) was added to FL-PTI^{n-} solution (8 mL, 0.5 mg·mL^{-1}), stirring with a glass stirrer bar for 10 min forming a slightly turbid pale yellow color of alkylated FL-PTI. The discharging and washing procedures was the same as set forth. Dodecane ($C_{12}H_{26}$, Sigma-Aldrich) was used in lieu of $C_{12}H_{25}Br$ in the control experiment.

5. Recovery of FL-PTI from the DMAc into aqueous solution:

The FL-PTI can be recovered from the solubilised FL-PTI$^{n-}{}_{(naphthalene/DMAc)}$ supernatant after centrifugation of PTI/NaNp/DMAc mixtures at 5000 *g* for 30 min by: (i) bubbling with dry air for 1 h and collecting the FL-PTI wet cake *via* vacuum filtration over a 20 nm pore AAO membrane (Whatman); (ii) sequential washing the wet-cake with copious amounts of tetrahydrofuran and ethanol to remove naphthalene and sodium salts, respectively. Care must be taken to ensure the material does not fully dry out between washings, which would re-introduce the heavy restacking; and (iii) re-dispersion in water by brief bath sonication (1 minute) with a saturated concentration of 3.5 mg·mL^{-1}.

6. Sonication synthesis of FL-PTI nanosheet suspension:

50 mg of PTI were dispersed in 20 mL of water. The ice-cooled suspension was sonicated for 6 h by a ultrasonic processor (Sonics, 750 W) with an amplitude of 40%. The resultant suspension was centrifuged (Sigma, 2-16K) at 5000 *g* for 30 min to obtain the brown-colored FL-PTI nanosheet suspension with a concentration of <0.2 mg·mL^{-1}.

7. Characterization:

Various microscopes, including two field emission transmission electron microscopes (FEI Titan and JEOL 2100F) and a tapping-mode atomic force microscopy (AFM, Bruker MultiMode 8) were used to characterize the exfoliated FL-PTI nanosheets. The FEI Titan, equipped with an aberration corrector, was operated at 80 kV and used to obtain HRTEM images. The JEOL 2100F, equipped with an Oxford 80mm X-Max EDX detector, was operated at 200 kV and used for EDX mapping. TEM and AFM of FL-PTI^{n-} (from supernatant after centrifugation at 5000 g for 30 min) and the insoluble fragment (from precipitate after centrifugation at 5000 g for 30 min) samples were prepared *via* directly drop-casting of anhydrous DMAc diluted FL-PTI$^{n-}_{(naphthalene/DMAc)}$ supernatant/insoluble precipitate on a 300 mesh Au holey carbon grid with an ultrathin 3 nm carbon support (Agar Scientific AG01824G) and freshly cleaved mica surface, respectively, followed by vacuum-drying at RT for 2 days under N_2. Then the samples were further washed sequentially with THF, water and acetone to remove the naphthalene and formed sodium hydroxide[4] with subsequent oven-drying at 100 ˚C overnight. The FL-PTI specimens for TEM and AFM were made by drop-casting of a dilute FL-PTI methanol/water (volume ratio of 5:1) solution on corresponding substrates, respectively. For HRTEM, an average background subtraction filter is used to remove contributions from the amorphous carbon substrate.[5] For AFM, the thicknesses of 206 FL-PTI nanosheets were measured, among which 169 were less than or equal to 14 Å, indicating that 82 % ≤ 4 layers based on a 3.52 Å layer thickness.[1] Thermogravimetric-mass spectroscopy (TGA, METTLER TGA-DSC 1) coupled with a mass spectrometer (MS, HPR-20 QIC) was performed under a well-controlled N_2 atmosphere. Typically, samples (~1.5 mg) were dried at 100 ˚C for 60 min and then heated to 800 ˚C at a ramp rate of 10 ˚C·min^{-1} under N_2 (60 s.c.c.m). UV-visible absorption spectra were recorded with a UV-vis spectrometer (Perkin Elmer Lambda 950) with an integration time of 0.5 s in an optical quartz cuvette with 1 cm pathlength. Specific surface areas were measured with a Micromeritics Tristar 3000 and calculated according to the Brunauer-Emmett-Teller (BET) equation from the adsorption isotherm. And the corresponding pore size distribution was calculated from desorption branch based on the Barrett-Joyner-Halenda method. Zeta potential (Malvern, Zetasizer Nano Series) was determined from a dilute FL-PTI aqueous solution with 10^{-3} wt% concentration. Hydrodynamic diameter of FL-PTI nanosheets were evaluated by dynamic light scattering (DLS, DelsaTM Nano C) at 25 ˚C. pH value of the nanosheet solution was measured based on a pH meter (Symphony, SB90M5) with a five point calibration system.

8. Density functional theory (DFT) modeling:

Density functional theory was adopted for the simulations, specifically the hybrid exchange-correlation B3LYP functional [6],[7] as implemented in the Crystal14 code.[8] 6-21G* Gaussian basis sets were employed. All species were treated at all-electron level. A Monkhorst-Pack shrinking factor of 6/6 was used, which led to 20 k-points in the irreducible Brillouin zone. Truncation thresholds were set to (6 6 6 6 12) for the Coulomb and exchange series. The SCF convergence criterion was set to 10^{-7} Hartree. The coordinates and computational cell parameters were fully optimized for all systems. Structure optimization was deemed converged when the largest component of gradient was 1.2×10^{-3} a.u. and of estimated nuclear displacement 1.8×10^{-3} a.u.. The optimised models of FL-PTI nanosheets with AB and AC stacking were used to simulate selected area electron diffraction (SAED) patterns, respectively.

9. X-Ray photoelectron spectroscopy (XPS):

All XPS spectra were recorded using a K-alpha$^+$ XPS spectrometer equipped with a MXR3 Al Kα monochromated X-ray source ($h\nu$ = 1486.6 eV). X-ray gun power was set to 72 W (6 mA and 12 kV). Charge compensation was achieved using the FG03 flood gun using a combination of low energy electrons and the ion flood source. Argon etching of the samples was done using the standard EX06 Argon ion source using 500 V accelerating voltage and 1 µA ion gun current. Survey scans were acquired using 200 eV pass energy, 1 eV step size and 100 ms (50 ms x 2 scans) dwell times. All high resolution spectra (N 1s, and Br 3d) were acquired using 20 eV pass energy, 0.1 eV step size and 1 second (50ms x 20 scans = 1000 ms) dwell times. Samples were prepared by pressing the sample onto double side sticky carbon based tape. Pressure during the measurement of XPS spectra was ≤ 1×10^{-8} mbar. Thermo Avantage software was used for data interpretation. Casa XPS software (version 2.3.16) was used to process the data. The quantification analysis was carried out after subtracting the baseline using the Shirley or two point linear background type. Peaks were fitted using GL(30) lineshapes; a combination of Gaussian (70%) and Lorentzian (30%). All XPS spectra were charge corrected by referencing the fitted contribution of C-C graphitic like carbon in the C1s signal 284.5 eV.

Results and Discussion

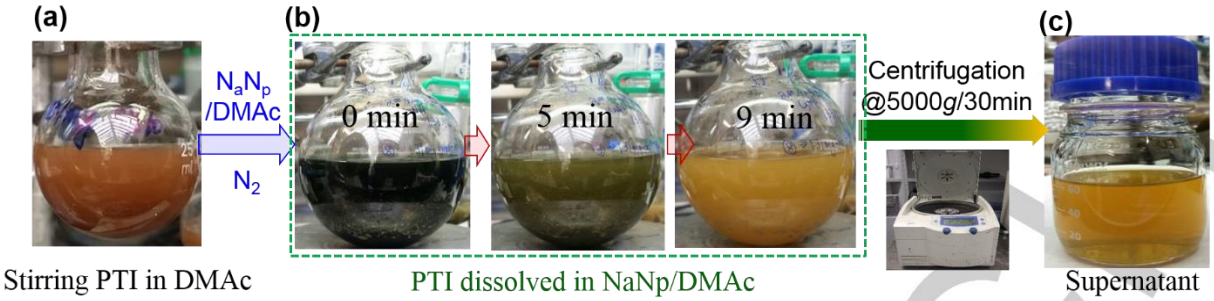

Figure S1. Sequential photographs of PTI suspension exfoliated in NaNp/DMAc solution with a simple magnetic stirring as time goes on.

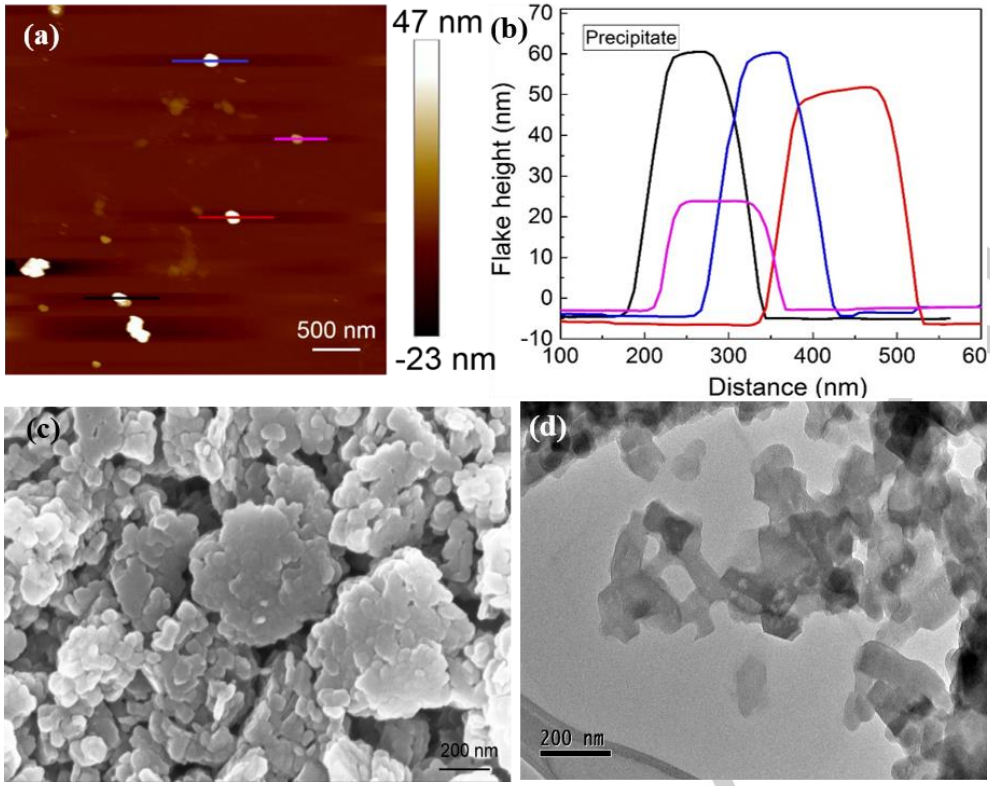

Figure S2. (a) AFM image and (b) corresponding height of four random sheets of precipitate after centrifugation at 5000 *g* for 30 min. (c) SEM and (d) STEM images of precipitate showing the insoluble fractions removed by centrifugation are still PTI. Similar to SWCNT dissolved in Na-ammonia solution[4] and graphite intercalation compounds dissolved in Na/naphthalene/THF solution,[9] which has the maximum yields of 15 and 24 wt% of the original samples, respectively, the remaining undissolved PTIs are likely to be caused either by inappropriate charging or physical trapping from defects.[4]

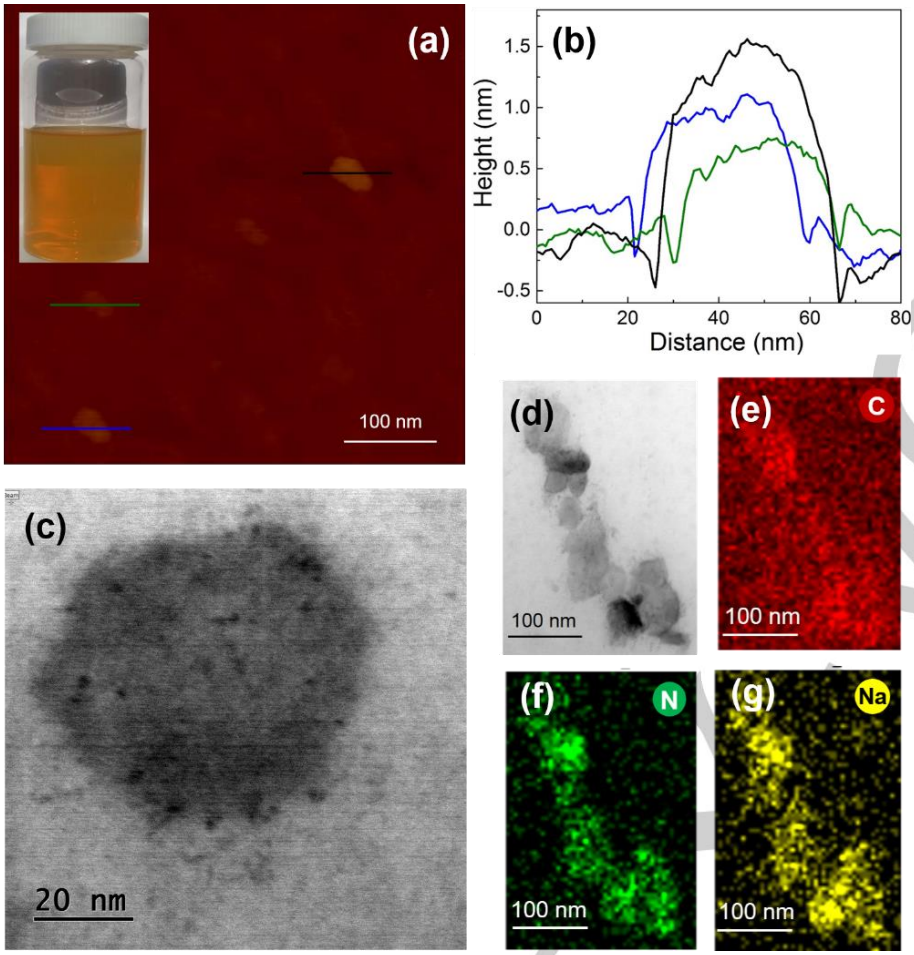

Figure S3. (a) AFM image of FL-PTI^{n-} nanosheets deposited on mica from DMAc solution. Inset: Photograph of FL-PTI$^{n-}{}_{(naphthalene/DMAc)}$ solution after being stored under N_2 for 1 year (7:1 PTI:Na ratio). (b) The corresponding height profile of three FL-PTI^{n-} nanosheets in AFM image. (c) STEM image of exfoliated hexagonal FL-PTI^{n-} nanosheet. (d) STEM image and EDX elemental maps of C (e), N (f) and Na (g) on Na doped FL-PTI^{n-} nanosheets. The background C signal in (e) is due to the carbon TEM support.

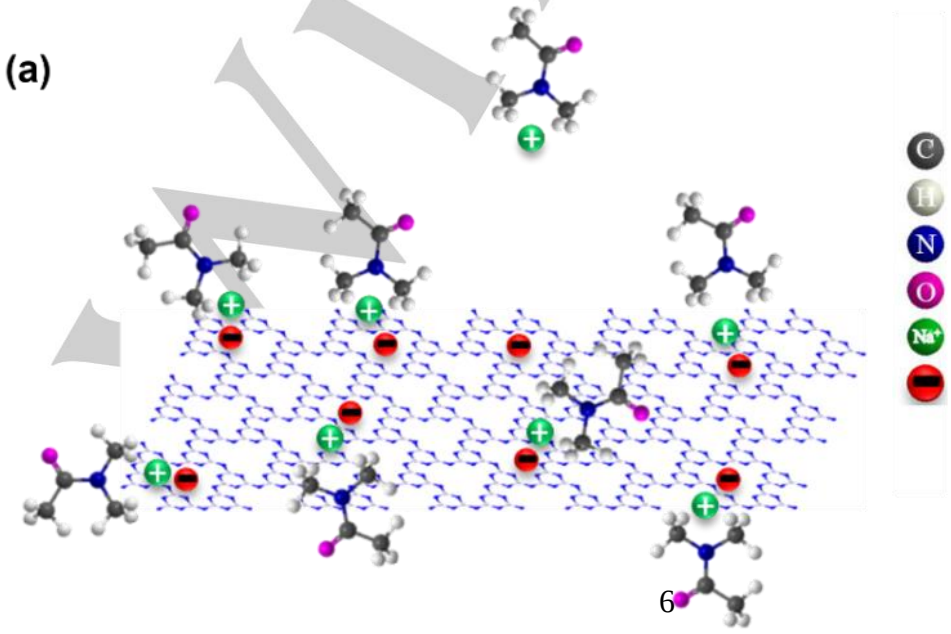

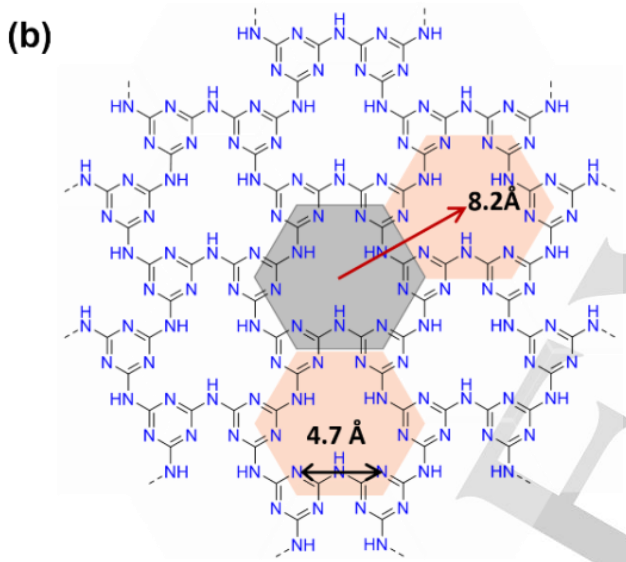

Figure S4. (a) Sketch of a FL-PTI^{n-} nanosheet with surrounding Na^+ in DMAc (naphthalene is omitted for clarity) and (b) a simplified PTI crystallographic structure.

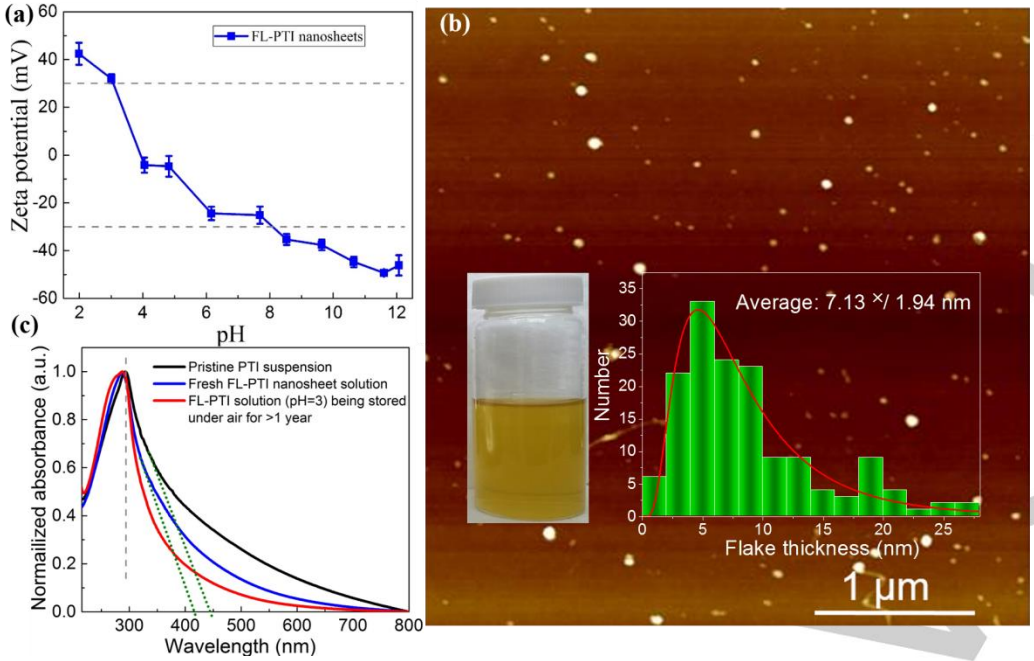

Figure S5. (a) Zeta potential of FL-PTI nanosheet aqueous solution as a function of pH. (b) AFM image of FL-PTI nanosheets deposited on mica from aqueous solution (at pH 7.7) being stored in air for 2 months. Inset: Dissolved FL-PTI nanosheet aqueous solution (7:1 PTI:Na ratio) exposed to air for 2 months (left) and statistical analysis of the thickness of ~150 FL-PTI nanosheets measured in AFM images (right). Mean value is derived from a lognormal distribution. The average flake height increases from 1.11 nm (Figure 3a, b) for the fresh FL-PTI nanosheet solution to 7.13 nm after exposed to air for 2 months (pH 7.7), demonstrating the slow reagglomeration on discharging with air exposure. (c) UV-visible absorption spectra of pristine PTI suspension, freshly exfoliated FL-PTI by framework charging method and FL-PTI aqueous solution (pH=3) after being stored in air for > 1 year.

As for the sonication exfoliated counterpart,[10] the FL-PTI aqueous dispersions are highly stable both at low (≤3) and high (≥8) pH ranges, where $|\zeta| \geq 30$ mV, generally considered sufficient to sustain mutual repulsion in colloids (Figure S5a).[11] Zeta potential measurements also show that the surface charge switches from negative (-49.5 ± 1.6 mV) to positive (+43.9 ± 3.3 mV) on decreasing the pH from 12 to 2, with an isoelectric point of pH 3.9 (Figure S5a), corresponding to the ionization and protonation of the bridged imide moieties within the PTI framework, respectively.[10,12] Adjusted the effective charge provides a feasible route to make PTI multifunctional macro-constructs *via* electrostatic self-assembly.[13] Moreover, the intrinsic absorption edge of ultrathin FL-PTI nanosheet solution shows a remarkable blue shift compared to its bulk counterpart (Figure S5c), corresponding to an increase in the band gap from 2.79 eV for bulk PTI to 2.99 eV for FL-PTI nanosheets, due to a possible quantum confinement effect.[14],[15] Meanwhile, the stability of the nearly overlapping UV-visible absorption feature at 287 nm, over time, excludes any ongoing aggregation in the FL-PTI solution.[3] The DLS result indicates a hydrodynamic diameter of pristine PTI is 1097 nm (90%), which decreases to only 226 nm (100%) for FL-PTI nanosheets immediately after framework charging exfoliatation,[10] with no significant change after keeping in air over 1 year when pH value of the PTI nanosheet solution is adjusted to 3 (280 nm, 100%), thus, confirming the excellent stability of as-prepared FL-PTI aqueous solution at both low (≤3) and high (≥8) pH ranges (Figure S5a).

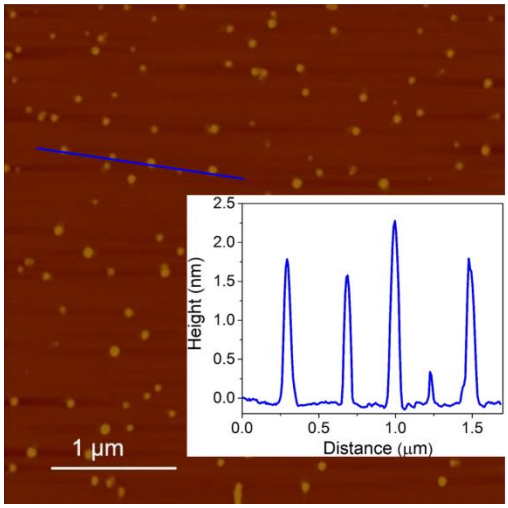

Figure S6. The corresponding height profile of five FL-PTI nanosheets along the blue line in AFM image.

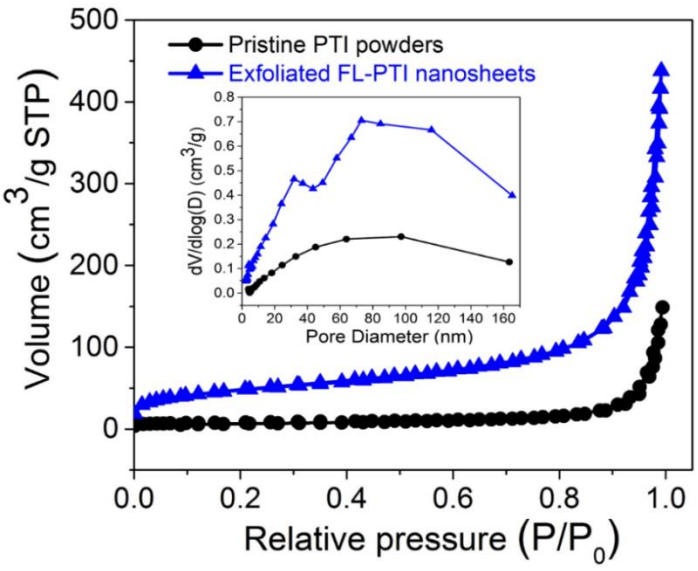

Figure S7. N_2 adsorption-desorption isotherms of pristine PTI and FL-PTI nanosheets. Inset: The corresponding pore size distribution curves. The 7-fold increase in BET specific surface area from 26 (bulk PTI) to 175 $m^2 \cdot g^{-1}$ (FL-PTI nanosheets), confirms significant exfoliation, but is limited by restacking during oven drying. Moreover, the FL-PTI has smaller pore sizes with peaks at 4, 32 and 73 nm, indicative of hierarchical pores compared to the pristine PTI powders which has a broad ranging from tens of nanometers to over one hundred nanometers.

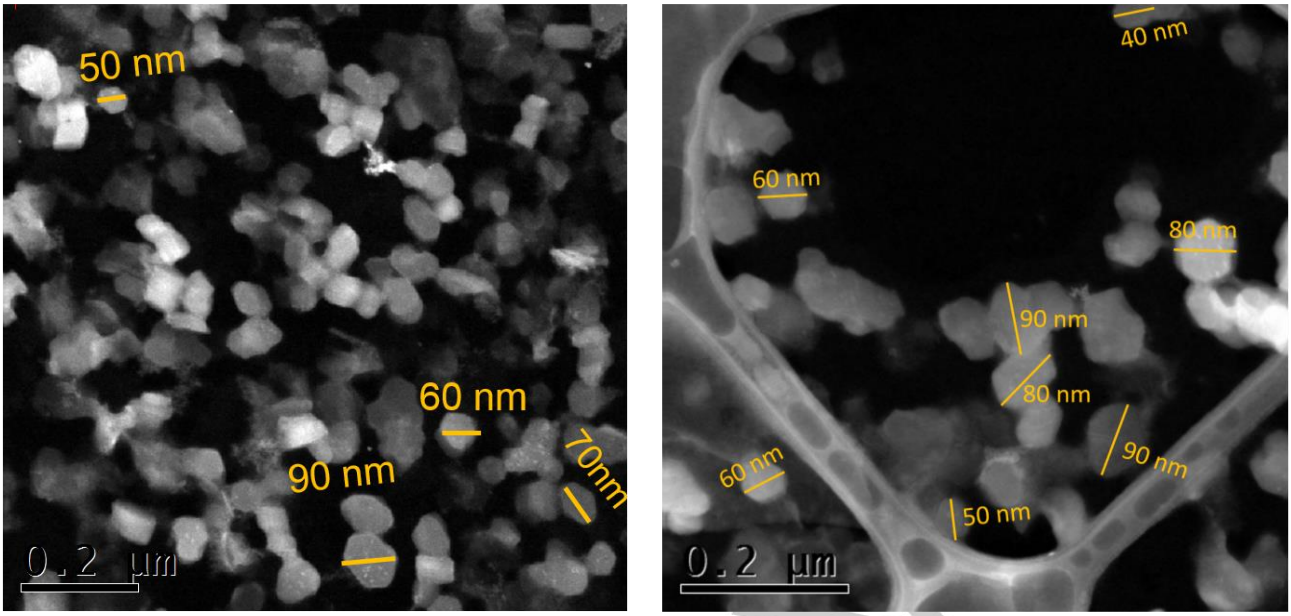

Figure S8. STEM images showing the lateral size of FL-PTI nanosheets.

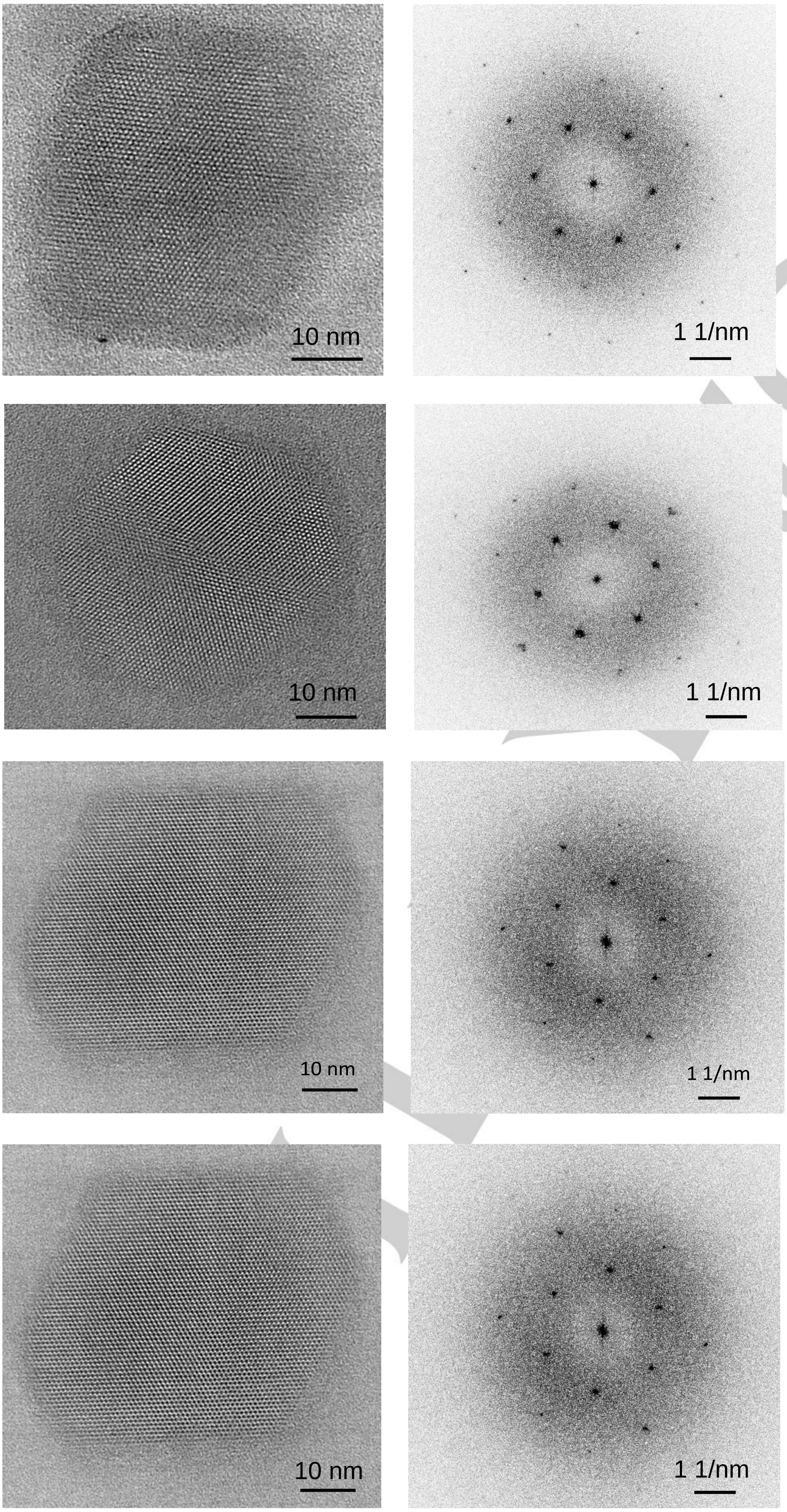
10 nm
1 1/nm
10 nm
1 1/nm
10 nm
1 1/nm
10 nm
1 1/nm

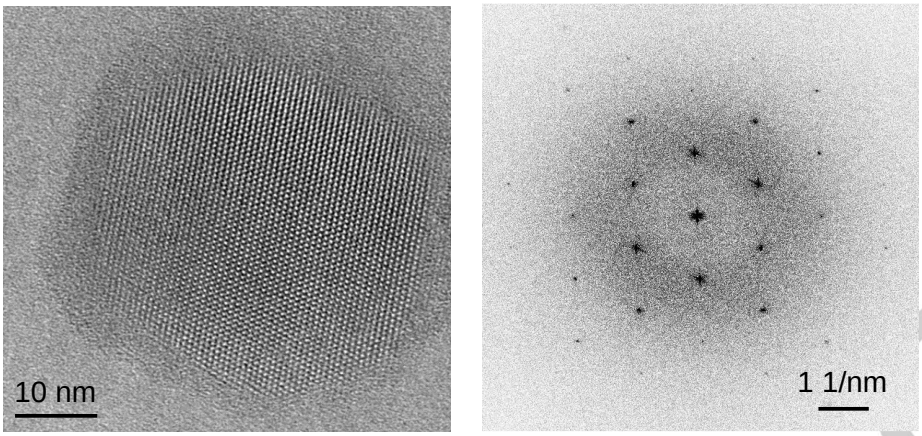

Figure S9. Supplemental HRTEM images (with an average background subtraction filter applied) and corresponding (unfiltered) FFTs of FL-PTI nanosheets, indicating single crystals with intact hexagonal lattice structure of FL-PTI nanosheets.

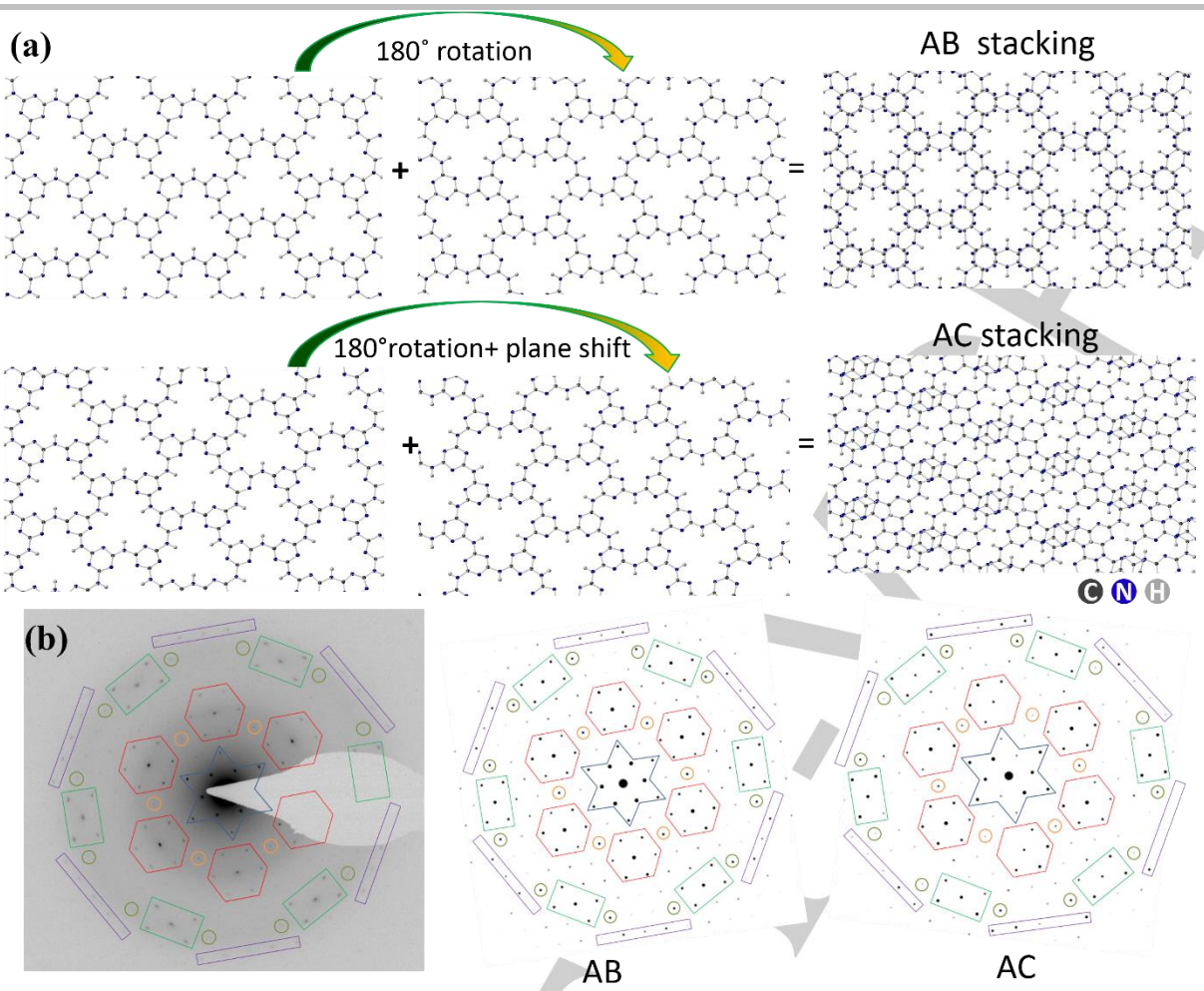

Figure S10. (a) Schematics of the two stacking structures, AB (top) and AC (bottom). DFT calculations show that in complete absence of intercalated anions FL-PTI stacks in the AC model shown here. However, the preferred stacking changes to AB with any amount of intercalated Cl^-/ Br^- ions, consistent with the reported bromide anions intercalated PTI strucutre.[1] (b) SAED pattern (left), and simulated electron diffraction patterns based on the AB (center) and AC (right) stacking structures. Qualitatively, the AB simulation reproduces the SAED data better than the AC simulation. The AB simulation has approximate 6-fold rotational symmetry and weak/absent diffraction peaks that match the SAED data, while the AC simulation does not. The colored star, hexagons, rectangles, and circles drawn on the SAED data and the simulations are guides to show these features more clearly. While the SAED data and AB simulation do not match quantitatively, this may be expected as structure factor determination in 2D materials is sensitive to the number of layers.[16]

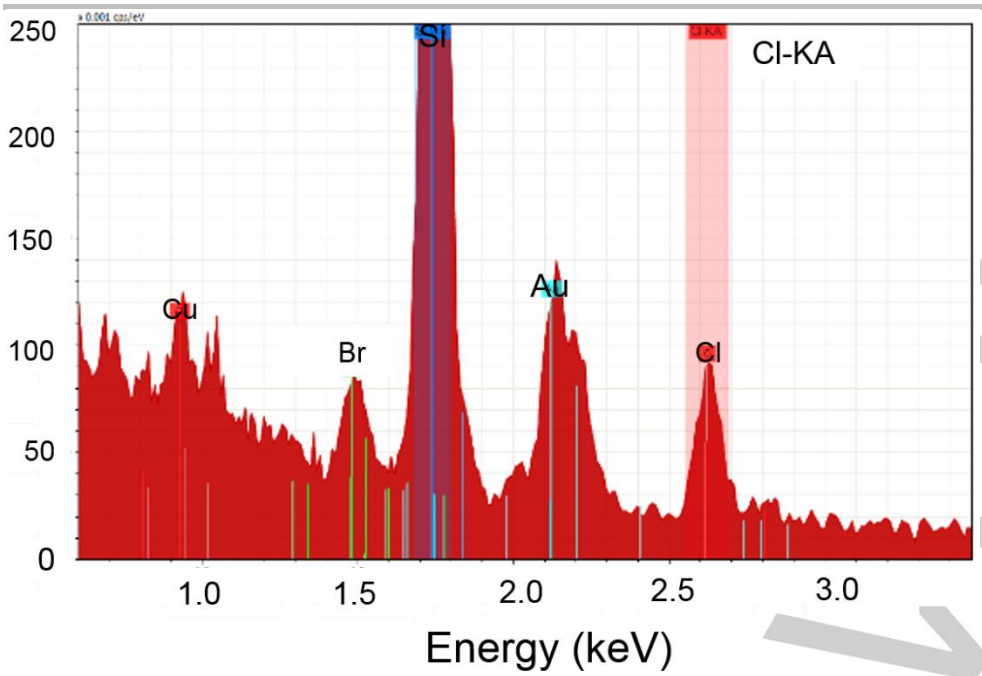

Figure S11. Partial EDX spectra of the FL-PTI nanosheet of Figure 3 showing trace amounts of Br and Cl.

Since no Cl was used in the processing of the FL-PTI nanosheets we attribute the Cl signal to background on the TEM grid (Cl was also detected on a blank grid). Br is thus likely stabilizing the AB stacking demonstrated in Figure S10. Here, the N:Br atomic ratio is ~700:1, corresponding to one intercalated Br^- anion per ~40 unit cells considering that one unit cell contains 18 N atoms. A FL-PTI nanosheet with ~90 nm lateral size (Figure S8) has ~30,000 unit cells per bilayer, and hence ~800 intercalated Br^- anions per bilayer. Since the presence of any Br^- intercalant stabilizes the AB stacking,[1],[2] and our FL-PTI nanosheets contain >> 1 Br^- intercalant anions per bilayer, the trace amount of Br detected may explain the observed AB stacking structure.

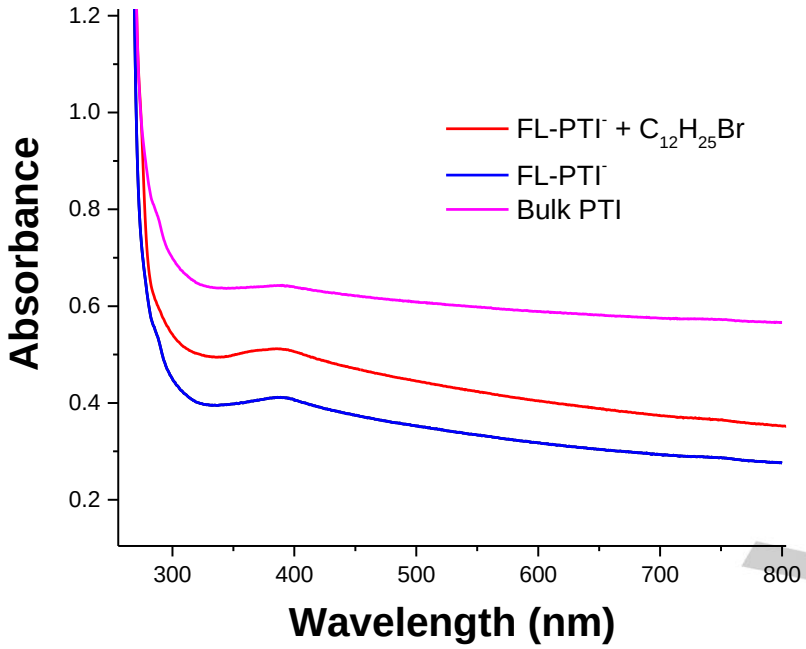

Figure S12. UV-vis spectra of FL-PTI$^-$, FL-PTI$^-$ + $C_{12}H_{25}Br$ and bulk PTI. Solution concentration is 100 µg/mL in dimethylacetamide for all the samples.

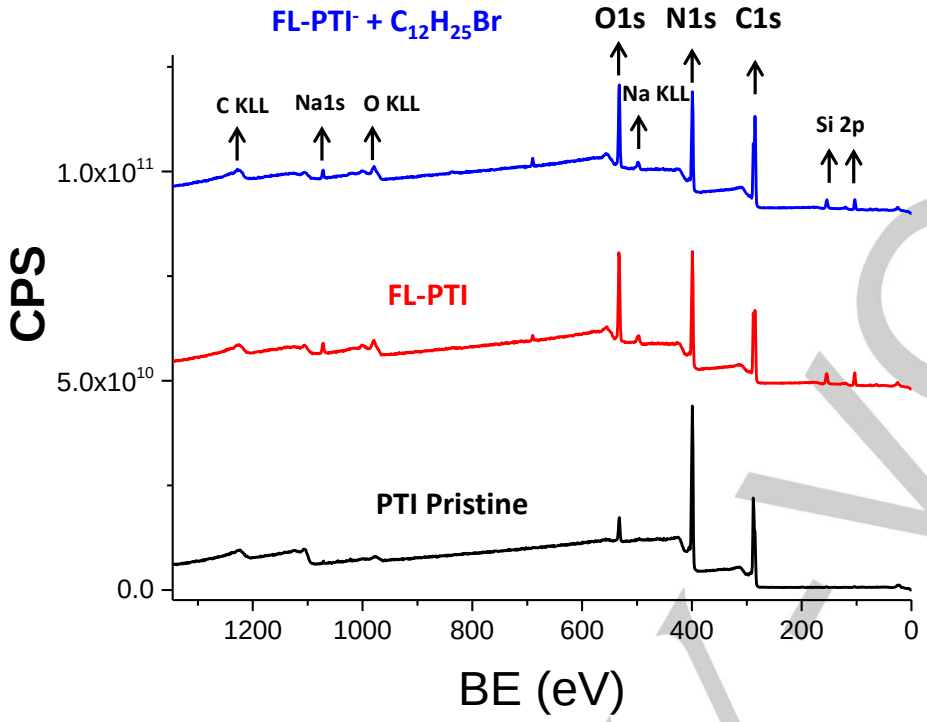

Figure S13. XPS Survey spectra of bulk PTI, FL-PTI and FL-PTI functionalised with dodecylbromide.

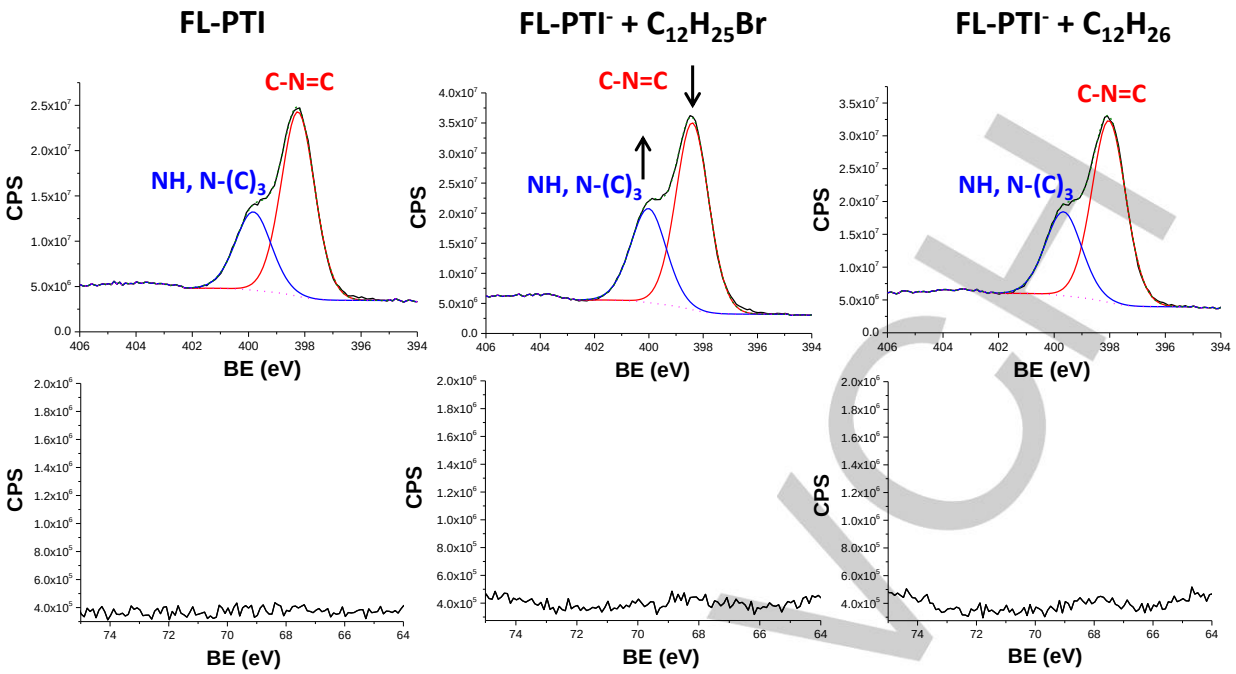

Figure S14. Core level N 1s (top panel) and core level Br 3d (bottom panel) of FL-PTI, FL-PTI functionalised with bromododecane, and control FL-PTI processed with dodecane

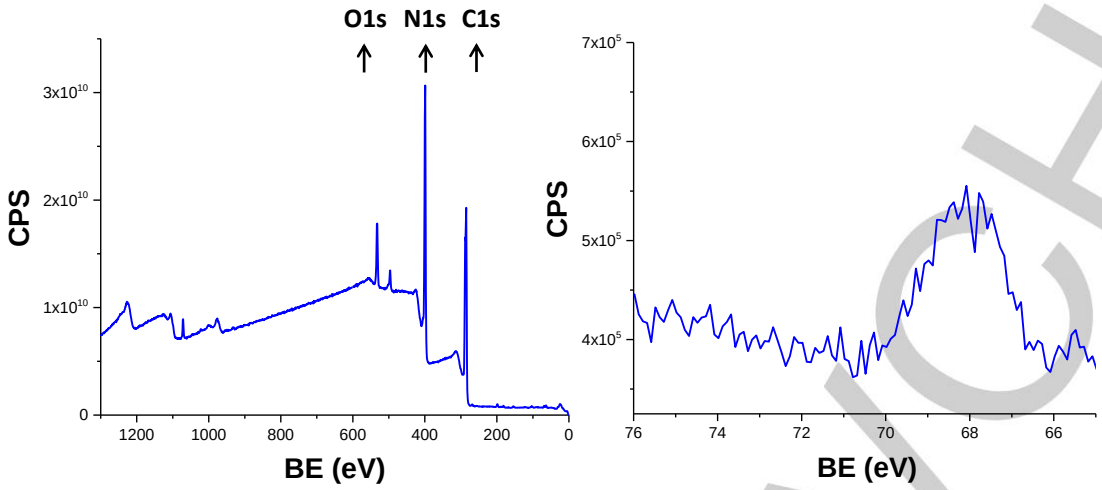

Figure S15. Survey and core level Br 3d scans of the physical mixture FL-PTI and $C_{12}H_{25}Br$.

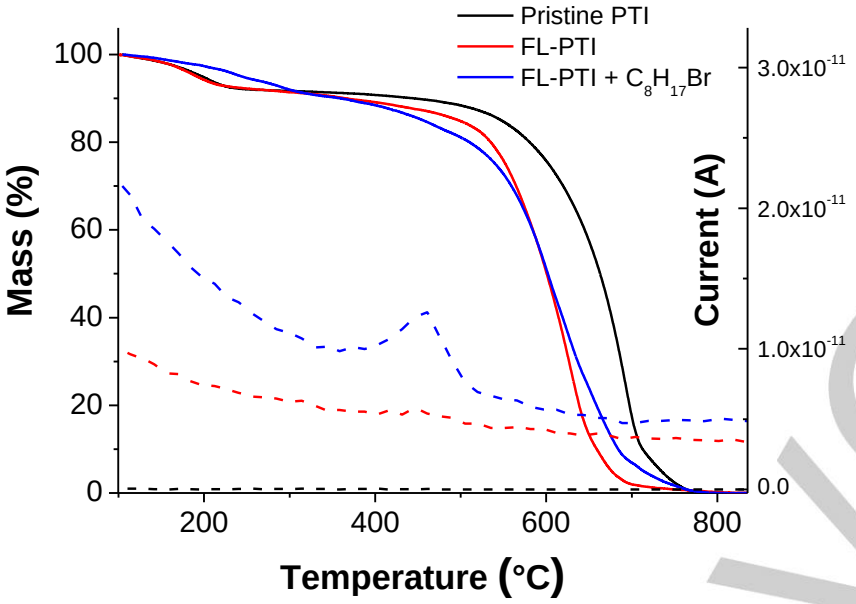

Figure S16. TGA-MS curves of Pristine PTI and FL-PTI$^-$ + $C_8H_{17}Br$. MS showing a weight loss from the moiety of $C_4H_9^+$ (m/z=57) due to the grafted C_8H_{17} alkyl chain (dashed line). This fragment is not present in Pristine PTI.

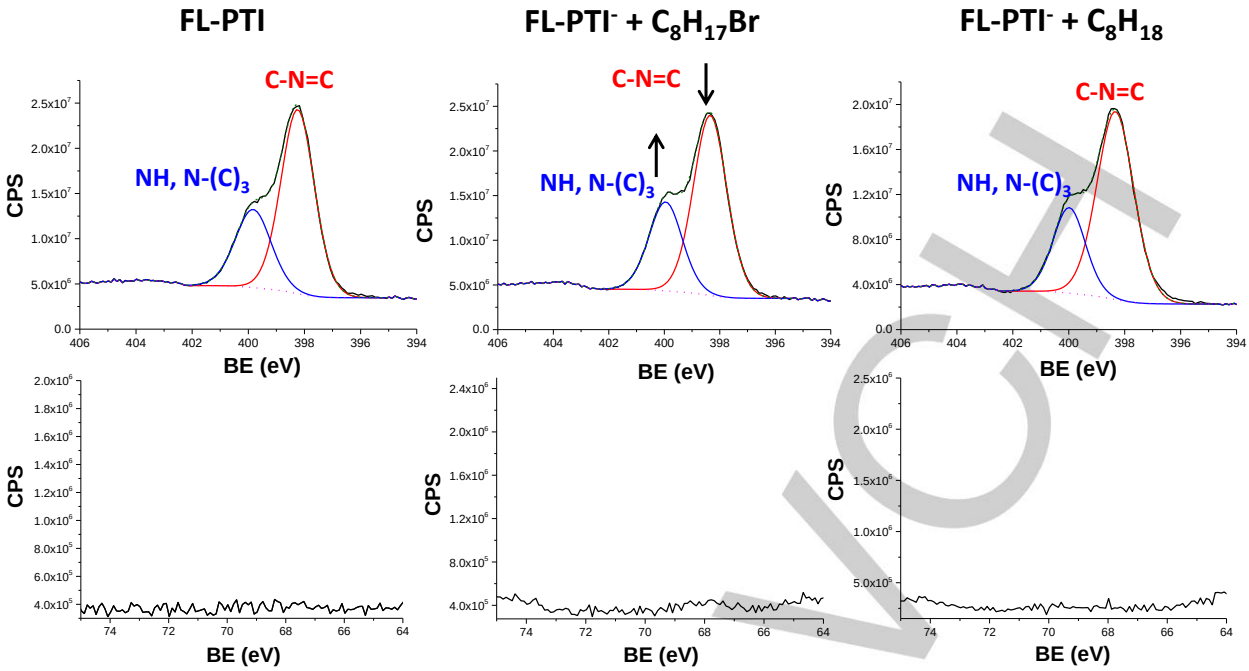

Figure S17. Core level N 1s (top panel) and core level Br 3d (bottom panel) of FL-PTI, FL-PTI functionalised with bromooctane and control processs FL-PTI and octane.

Table S1. Quantitative analysis of the components that form the N 1s peak

Sample	C-N=C component (%)	NH/N-$(C)_3$ component
Pristine PTI	64.1 ± 0.2	35.9 ± 0.2
FL-PTI nanosheets	67.6 ± 0.3	32.4 ± 0.3
FL-PTI⁻ + $C_{12}H_{25}Br$	65.1 ± 0.7	34.9 ± 0.7
FL-PTI⁻ + $C_{12}H_{26}$	67.7 ± 0.8	32.4 ± 0.8
FL-PTI⁻ + $C_8H_{17}Br$	64.1 ± 1.2	35.9 ± 1.2
FL-PTI⁻ + C_8H_{18}	69.1 ± 0.7	30.9 ± 0.7

PTI layers were functionalised with deuterated ethyl chains in an attempt to characterise this sample with solid state NMR (ssNMR):

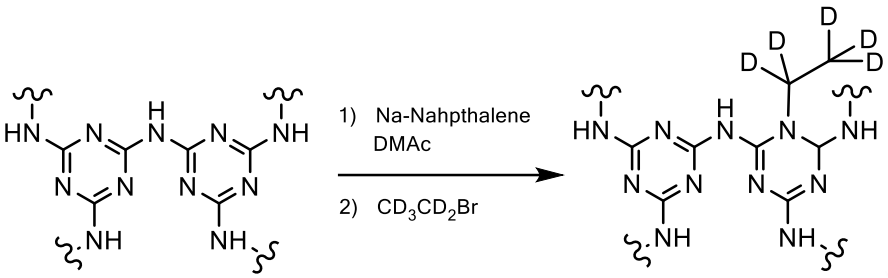

Scheme S1. Reaction between PTI and deuterated bromo-ethane.

Unfortunately, the ssNMR was still not sufficiently sensitive to detect the deuterated signal. However, the deuterated sample did provide another useful confirmation of functionalisation. TGA-MS confirmed the presence of the deuterated chains at 450ºC (m/z = 34, CD_3-CD_2^+). The other functionalised samples (e.g. FL-PTI$^-$ + $C_8H_{17}Br$) did not show this fragment, confirming that the fragment m/z = 34 is due to the grafting of deuterated chains only.

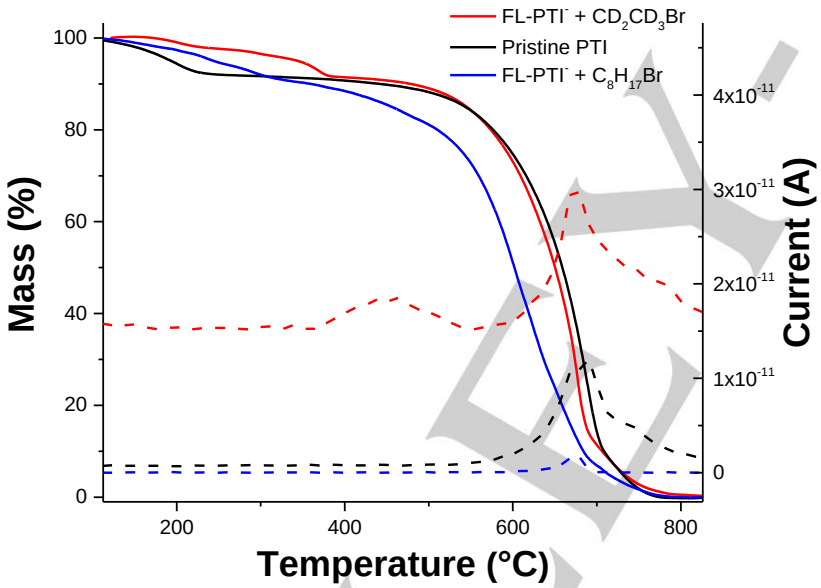

Figure S18. TGA-MS of FL-PTI$^-$ + CD_2CD_3Br.

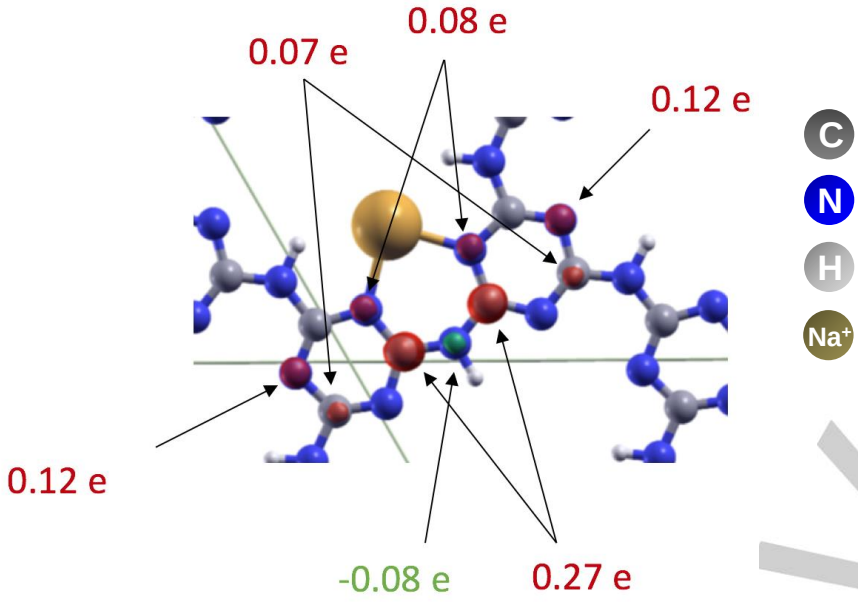

Figure S19. DFT optimised orbital structures of PTI-Na.

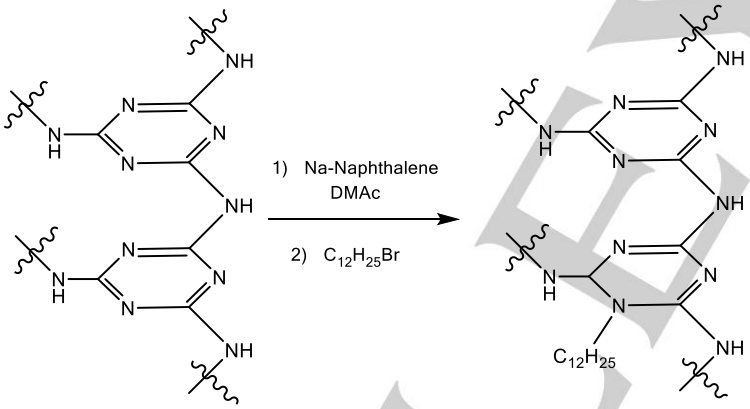

Scheme S2. Proposed reaction of PTI charging and functionalisation process.

References

[1] S. Y. Chong, J. T. A. Jones, Y. Z. Khimyak, A. I. Cooper, A. Thomas, M. Antonietti, M. J. Bojdys, *J. Mater. Chem. A* **2013**, *1*, 1102-1107.

[2] E. J. McDermott, E. Wirnhier, W. Schnick, K. S. Virdi, C. Scheu, Y. Kauffmann, W. D. Kaplan, E. Z. Kurmaev, A. Moewes, *J. Phys. Chem. C* **2013**, *117*, 8806–8812.

[3] A. J. Clancy, J. Melbourne, M. S. P. Shaffer, *J. Mater. Chem. A* **2015**, *3*, 16708–16715.

[4] S. Fogden, C. A. Howard, R. K. Heenan, N. T. Skipper, M. S. P. Shaffer, *ACS Nano* **2012**, *6*, 54–62.

[5] R. Kilaas, *J. Microsc.* **1998**, *190*, 45–51.

[6] A. D. Becke, *J. Chem. Phys.* **1993**, *98*, 5648–5652.

[7] S. H. Vosko, L. Wilk, M. Nusair, *Can. J. Phys.* **1980**, *58*, 1200–1211.

[8] R. Dovesi, R. Orlando, A. Erba, C. M. Zicovich-Wilson, B. Civalleri, S. Casassa, L. Maschio, M. Ferrabone, M. De La Pierre, P. D'Arco, Y. Noël, M. Causà, M. Rérat, B. Kirtman, *Int. J. Quantum Chem.* **2014**, *114*, 1287–1317.

[9] T. Morishita, A. J. Clancy, M. S. P. Shaffer, *J. Mater. Chem. A* **2014**, *2*, 15022-15028.

[10] K. Schwinghammer, M. B. Mesch, V. Duppel, C. Ziegler, J. Senker, B. V. Lotsch, *J. Am. Chem. Soc.* **2014**, *136*, 1730–1733.

[11] D. Li, M. B. Müller, S. Gilje, R. B. Kaner, G. G. Wallace, *Nat. Nanotechnol.* **2008**, *3*, 101–5.

[12] Y. Zhang, A. Thomas, M. Antonietti, X. Wang, *J. Am. Chem. Soc.* **2009**, *131*, 50–51.

[13] W. J. Ong, L. L. Tan, S. P. Chai, S. T. Yong, A. R. Mohamed, *Nano Energy* **2015**, *13*, 757–770.

[14] X. Zhang, X. Xie, H. Wang, J. Zhang, B. Pan, Y. Xie, *J. Am. Chem. Soc.* **2013**, *135*, 18–21.

[15] P. Niu, L. Zhang, G. Liu, H. M. Cheng, *Adv. Funct. Mater.* **2012**, *22*, 4763–4770.

[16] B. Shevitski, M. Mecklenburg, W. A. Hubbard, E. R. White, B. Dawson, M. S. Lodge, M. Ishigami, B. C. Regan, *Phys. Rev. B - Condens. Matter Mater. Phys.* **2013**, *87*, 045417.

Complete Reference in Main Text:

[3] N. Mansor, T. S. Miller, I. Dedigama, A. B. Jorge, J. Jia, V. Brázdová, C. Mattevi, C. Gibbs, D. Hodgson, P. R. Shearing, C. A. Howard, F. Corà, M. S. P. Shaffer, D. J. L. Brett, P. F. McMillan, *Electrochim. Acta* **2016**, *222*, 44–57.

[13] P. L. Cullen, K. M. Cox, M. K. B. Subhan, L. Picco, O. D. Payton, D. J. Buckley, T. S. Miller, S. A. Hodge, N. T. Skipper, V. Tileli, C. A. Howard, *Nat. Chem.* **2016**, DOI 10.1038/nchem.2650.

[21] J. Yuan, J. Wu, W. J. Hardy, P. Loya, M. Lou, Y. Yang, S. Najmaei, M. Jiang, F. Qin, K. Keyshar, H. Ji, W. Gao, J. Bao, J. Kono, D. Natelson, P. M. Ajayan, J. Lou, *Adv. Mater.* **2015**, *27*, 5605–5609.